CHAPTER - 5

Elastic Scattering and total reaction cross section with radioactive ion beam

Published in:

1. S. Mukherjee, **N. N. Deshmukh** *et al., Total reaction cross-sections for light weakly bound systems*, Eur. Phys. J A **45**, 23 – 28 (2010).

5.1 Introduction

It is well known that the properties of nuclei far from the stability valley differ in many aspects from those of ordinary nuclei [1–9]. The peculiarities of nuclear forces and many-body systems make probable the existence of both light and heavy weakly bound nuclei with a diffuse surface layer. The correlations of the valence neutrons and the strong coupling with the continuum can significantly distort the shell structure as well as the collective properties of the weakly bound asymmetric nuclei with $N > Z$. Effects due to these properties should be expected also in the dynamics of the reactions induced by these nuclei. With the improvement of radioactive ion beam (RIB) acceleration techniques, it has become possible to produce variable energy, relatively intense beams of radioactive nuclei in a wide range of N and Z. The use of secondary beams of radioactive nuclei considerably widens the possibilities to investigate the properties of atomic nuclei and nuclear reactions. There are three main issues of nuclear physics to be addressed in the experiments involving short-lived radioactive ion beams: the investigation of the properties of the atomic nuclei far from the stability line, the study of the peculiarities of the dynamics of nuclear reactions induced by proton- and neutron-rich nuclei and the synthesis and properties of new elements and isotopes.

The low-energy reactions of few-nucleon transfer induced by radioactive beams open up new possibilities to investigate the cluster structure and to obtain the spectroscopic characteristics of short-lived nuclei [10–12]. Also of great interest are some other reactions mechanism induced by radioactive nuclei such as elastic scattering, fusion and breakup. These reaction mechanisms are closely correlated and give new information both on the structure of the weakly bound nuclei and on the nuclear dynamics in which they participate. The elastic scattering of light exotic nuclei gives information on the nucleus-nucleus interaction of systems far from stability, which are characterized by large isospin and strong coupling to the continuum, namely the breakup channel of the weakly bound nucleus. The parameters of this interaction are of interest not only by themselves, but also they are necessary for analysis and understanding of the dynamics of more complicated reactions (fusion, breakup and few-nucleon transfer reactions).

It is of considerable interest to study the elastic scattering on light, medium and heavy targets that play a leading role towards the understanding of the dissociation of the weakly bound systems. From this, it is important to study the elastic scattering on different projectile target combinations with varying asymmetry, in order to understand more complicated reactions. The cross-section of elastic scattering can help to obtain an optical potential which is necessary to understand the entrance and exit channel potentials of some transfer reactions. Breakup effects also play an important role in the scattering mechanism, affecting the interaction potential. One of the important points of investigation is whether the effect of breakup is essentially to increase the total reaction cross-section. Therefore, it is important to investigate the dependence of the breakup and total reaction cross-sections on the breakup threshold for different projectiles on light- and medium-mass targets.

In the present work we investigate total reaction cross sections for a variety of systems consisting on weakly, tightly bound (stable) and radioactive proton or neutron halo projectiles on light targets. As has been shown in previous works [13–15] the total reaction cross-sections for the proton halo ^{8}B are larger than for no-halo projectiles. Here we are particularly interested in the investigation of total reaction cross-sections induced by its mirror nucleus, ^{8}Li. The ^{8}Li nucleus is radioactive and decays to ^{7}Li + n with a separation energy of 2.033 MeV which is much higher than the one for the ^{8}B nucleus (0.137 MeV) and similar to the ones of the stable weakly bound isotopes ^{6}Li (1.48 MeV) and ^{7}Li (2.45 MeV). It is therefore interesting to investigate whether its total reaction cross-section on different targets behaves more like to reactions induced by ^{8}B mirror or to the stable isotopes ^{6}Li and ^{7}Li, as there were not too many data available for reactions induced by this projectile in literature. There are only one energy point measurement available for the ^{8}Li + ^{51}V [16] system and two energy point measurements available for the ^{8}Li + ^{9}Be system [17, 18]. Moreover, there is a wide energy gap of 13 MeV between the earlier measurements in the ^{8}Li + ^{9}Be system. Therefore, we have measured some extra elastic scattering angular distributions for the ^{8}Li + ^{9}Be and ^{8}Li + ^{51}V systems at the incident energies, 19.6 MeV and 18.5 MeV, respectively, in order to complement the present data with the previous experimental data.

For a systematic study of reaction cross-sections, a direct comparison of data with theoretical predictions for each system is not very convenient since different systems would be distorted by differences like the projectile's charge or/and size. It is then necessary to reduce the data in a way that the influence of such factors would be washed out. For this purpose, different proposals can be found in the literature. A few years ago a reduction method was proposed that has been widely used [19]. However, very recently a new reduction procedure was proposed [20] for the study of fusion of weakly bound nuclei and later extended to total reaction cross-sections [13]. These methods lead to somehow different results for several projectiles on the ^{27}Al target [13, 21]. In the present work we compare the results using both the methods for the systems investigated, namely, ^{8}Li + ^{9}Be,^{51}V.

5.2 Details of Radioactive Ion Beam Production

The experiment with radioactive beam presented in this chapter were performed in the system RIBRAS [22, 23] (Radioactive Ion Beams in Brazil), at University of São Paulo, São Paulo, Brazil (Fig. 5.1). This apparatus is equivalent to TwinSol [24] at the laboratory of Notre Dame. RIBRAS system consists of a pair of superconducting solenoids that are capable of separating ions and produce beams of radioactive nuclei. The characterization of the profile of secondary beams produced in RIBRAS was made using a detector PPAC (parallel plate avalanche counter) [25].

5.2.1. Radioactive Beams

Exotic nuclei can be studied with the use of secondary beams. The intensity and purity of these beams are relative and vary according to the particularity of each experiment. In general, an intensity greater than 10^4 particles / s is sufficient to work, and a secondary beam impure, even with many contaminants, it is acceptable if they do not interfere in the results of interest. There are several possible methods for the production of radioactive beams [26]. In general there exist two complementary ways to make good quality beams of exotic nuclei: (i) the in-flight separation technique and (ii) the isotope separation on line (ISOL) technique. A driver accelerator or reactor provides the particles inducing nuclear reactions in a target. In the in-Flight method the primary particles have to be heavy and energetic and the target has to be thin in order to have the reaction products recoiling out of the target (fission is an exception to the statement of heavy and energetic particles as the reaction also can be induced by photons, electrons and light particles; the energy released in fission is high enough for the fragments to leave the thin target). The In-Flight method is applicable to very short-living nuclei (μs) as only the flight time from the production target to the measuring station induces decay losses. With the In-Flight method the radioactive ions are energetic and can eventually be slowed down and stored. In the ISOL method the radioactive products have to be thermalized in a catcher and then re-accelerated. The resulting beams are ion-optically (emittance, energy resolution, timing structure) of excellent quality but the thermalization process and the eventual re-ionization in the ion source can be slow and even inefficient leading to severe losses for short-living nuclei or for isotopes from refractory elements. If the slowing down process happens in a gaseous catcher leaving the ions in a 1^+ charge state (eventually after re-ionization by resonant laser light), these deficiencies of the target-catcher-ion source systems in the conventional ISOL can be avoided. This is also the way how the best of both (In Flight and ISOL) worlds can be obtained and a high-quality beam of short-living radioactive ions can be produced.

The technique used for the production of radioactive beams in the system RIBRAS, is the transfer of nucleons in flight. The method enables the production of useful nuclei with very short half life ($\tau_{1/2} \approx 100$ns) and low energy (3-5MeV/u in the current assembly of RIBRAS after the Pelletron accelerator). In this process, a primary beam of low energy focuses on a target of production (also called the primary target) that will produce a secondary beam of radioactive nuclei by transfer reactions (one or two nucleons) with large cross sections. The radioactive ions are then separated by magnetic fields (if the RIBRAS) and / or electric. Despite producing nuclei not far from the line of stability (i.e. ± 1 or ± 2 nucleons), these are the most significant in the processes of stellar nucleosynthesis [27].

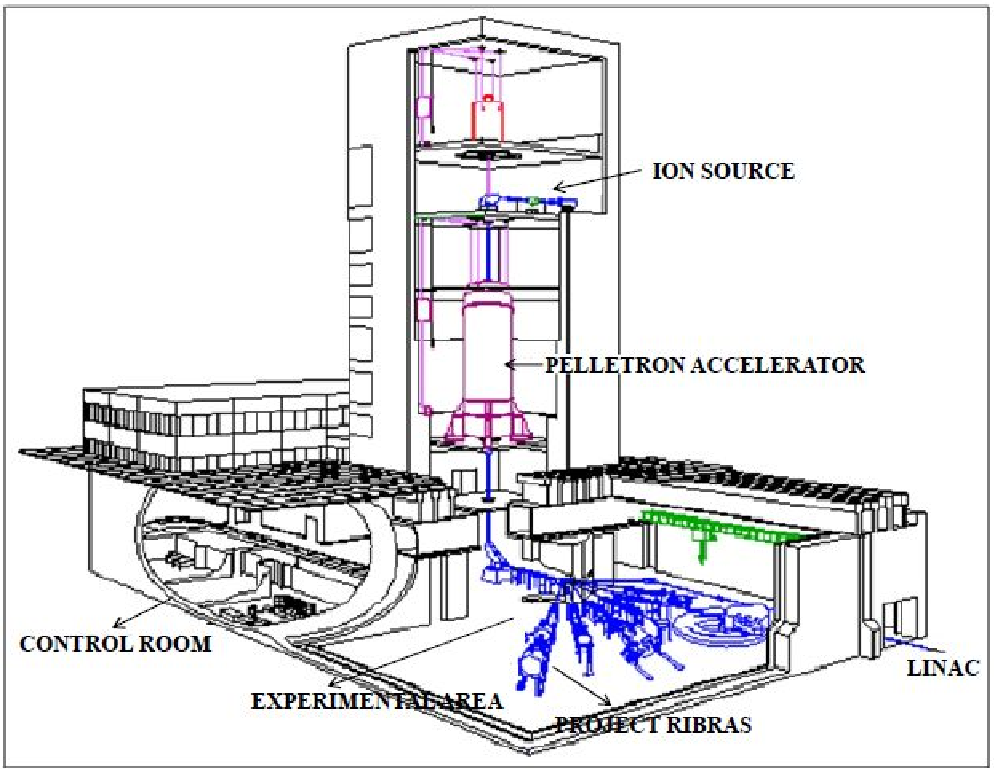

Figure 5.1: Overview of the Pelletron Laboratory of the Institute of Physics of the University of São Paulo, Brazil, RIBRAS system.

5.2.2 ION SOURCE

The source of ions MC-SNICS (Multi Cathode - Source of Negative Ions by Cesium Sputtering), built by National electrostatics Corporation (NEC), produces beams of negative ions or molecules.

In order to obtain beams of ^{6}Li and ^{7}Li, material containing these chemical elements and prepared, deposited and compressed in special crucibles of about 1mm in diameter, which are called cathodes. This source allows the assembly of up to 32 different cathode materials, allowing the change from one beam to another quickly and without the need to open the source and expose the air cathode. The output beam at the source is given by cesium ion bombardment of the material deposited on the cathode (Fig. 5.2). The cesium vapor, formed in the "heating" (container heated to 120 °C), enters through a valve in an area (ionization chamber) between the cathode and a cold surface ionizing heater (the ionizer).

A portion of the cesium is condensed on the surface of the cathode material and another part is positively ionized by ionizer surface. The cesium ionized particles are accelerated toward the cathode, colliding with the particles of the material which are ejected (sputtering). Some materials give off negative ions, while others expel neutral or positively charged particles. The latter captures the valence electrons of cesium condensed layer on the surface of the material, producing a beam of negative ions. This beam is then extracted from the source through a potential of 20 kV extractor. The beam current obtained in a Faraday cup for ^{7}Li ranged from 200 nA to 400 nA and for ^{6}Li was maintained at about 800 nA to 1μA.

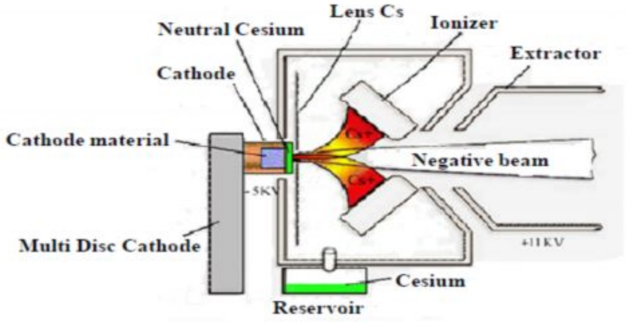

Figure 5.2: Schematic diagram of the sputtering process.

5.2.3 Pelletron Accelerator

Shortly after leaving the pre-accelerator tube, the beam contains a variety of ions produced at the source, of which only one is desired, in this case, ^{8}Li. The ions are selected by their mass (M), energy (E) and charge (Z) by the action of an electromagnet whose maximum value is ME/Z^{2} which is 20 (ME-20), which deflects the beam 90°, leaving it upright and directing it to the terminal of the accelerator.

The 8 UD Pelletron accelerator is an electrostatic machine, Tandem type with 8 MeV maximum voltage at the terminal. The charge of the terminal is produced by action on the inductive current of metallic cylinders (pellets) with insulating nylon links. A high voltage supply polarizes a negative inductor grounded near the pulley; this pushes the electrons out of the pellets as they are in contact with the pulley. Since the pellets remain on the action of the field of the inductor while leaving the pulley, they store an amount of positive charge. The present experiment was conducted by Dr. S. Mukherjee (thesis supervisor) using the above mentioned facility in Brazil. The details related to the RIBRAS machine can be found in references [16, 21, 28, and 29]. A detailed description of the present work is mentioned in the section 5.3 and in reference [30].

5.2.4. RIBRAS (Radioactive Ion Beam in Brazil)

The RIBRAS is a system composed of two superconducting solenoids installed in the pipe 45-B Pelletron-LINAC laboratory of São Paulo University, Brazil, that allows in-flight production of secondary beams of light radioactive nuclei of low-energy (energy of the secondary beam 2-10 MeV/u). This apparatus (Fig. 5.3) is capable of producing a wide variety of light beams, for example: ^{8}Li, ^{6}He, ^{7}Be, ^{8}B and ^{18m}F, with intensities ranging from 10^4-10^6 pps.

The first step in producing a secondary beam is the incidence of the primary beam on a target (primary target), producing the desired reaction. The primary target is in the center of the target chamber, about one meter from the center of the first solenoid. The system RIBRAS has a gas system that allows the use of targets or simply cooling gas to solid targets. Havar sheets are used to seal the windows for entry and exit of the target. The primary targets are embedded in the solid output window, keeping the entry window closed with a sealing sheet Havar. The cooling is usually done with helium gas, which can be done with air at a higher cost of energy degradation. Table 5.1 provides a list of examples of transfer reactions to produce nuclei far from stability line:

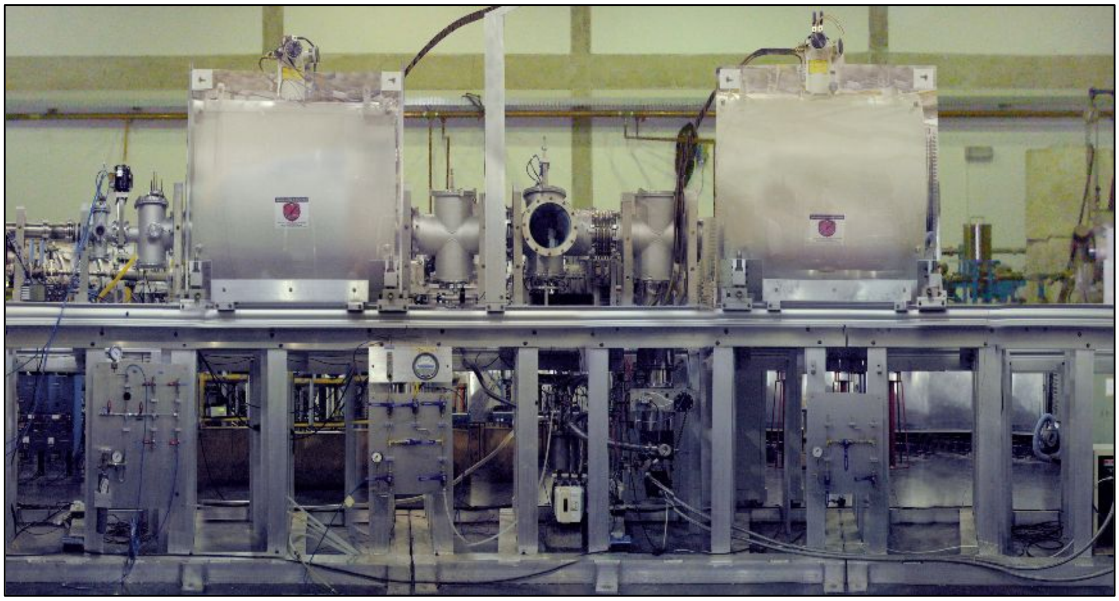

Figure 5.3: RIBRAS solenoid and target system for the production of radioactive ion beams.

Table 5.1 Possible radioactive ion beams obtained from the system RIBRAS.

Radioactive beam	**Production reaction**
^{8}Li	^{9}Be(^{7}Li,^{8}Li)^{9}Be [31]
^{6}He	^{9}Be(^{7}Li,^{6}He)^{10}B [31]
^{7}Be	^{3}He(^{6}Li,^{7}Be)d [31]
^{7}Be	^{3}He(^{7}Li,^{7}Be)t
^{8}B	^{3}He(^{6}Li,^{8}B)n
^{12}B	^{9}Be(^{7}Li,^{4}He)^{12}B [31]
^{18m}F	^{12}C(^{17}O,^{18m}F)^{11}B [31]

5.2.5. Electronics and Data Acquisition

The electronic assembly used in the experiments can be seen in Fig. 5.4. The voltage detector is supplied from two sources Quad Bias Supply ORTEC 710. The pulses generated by the silicon surface barrier detectors go through pre-amplifiers (models 142 PC-ORTEC and Canberra 2003BT), just outside the scattering chamber. The signals of the power outputs of the preamplifiers are sent to amplifiers ORTEC 572A, where the gain is adjusted and form (shapping time) of the bipolar pulses sent to the analog to digital converter (ADC 4418V-SILENA) of CAMAC (Computer Automated Measurement and Control / Model C111A) for further data processing.

The time signals are sent to a fast amplifier (ORTEC 820-FTA Fast Amp) and then transformed into a logic signal discriminator module Octal CF 8000 ORTEC. A logic module Fan in / Fan out (Lecroy Model-429A) receives the signals from all detectors generating a single signal at its output, which is transmitted to a module OGG (Octal Gate Generator) model – ORTEC module GG8010. The OGG generates a logic signal (adjustable) that serves as a trigger for the CAMAC system, warning of the occurrence of events. During this period, the CAMAC keeps the reading of unipolar pulses for ADC's and then processes them with the help of the module EH (Event Handler), previously programmed by the User.

The reading of the Faraday cup is formed by a current integrator (Digital Current Integrator ORTEC-429), transformed into logical pulses (416A Gate & Delay Generator-ORTEC) set in OGG and acquired by the scalar (LECROY, 2551) of CAMAC. The data is finally sent to the data acquisition system (Scan Root-Linux), which in addition to controlling the CAMAC is responsible for recording the data in the microcomputer acquisition.

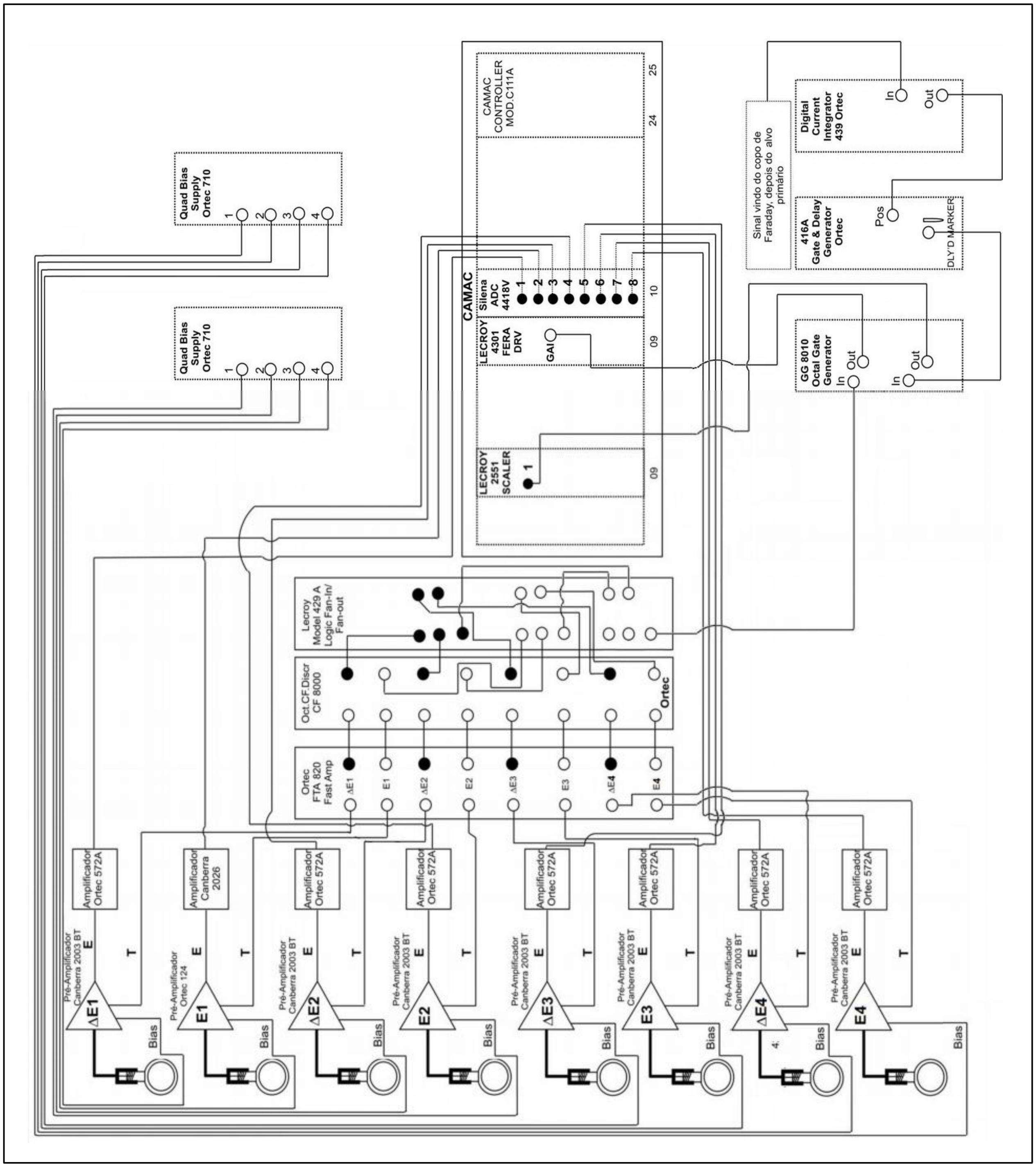

Figure 5.4: Electronics used in data acquisition.

5.3 Elastic scattering measurements for ^{8}Li + ^{9}Be, ^{51}V systems

The present elastic scattering experiments were performed by thesis supervisor, for the ^{8}Li + ^{9}Be and ^{8}Li + ^{51}V systems using the 8 UD Pelletron accelerator of the University of Sao Paulo, Brazil. The secondary radioactive ion beam ^{8}Li was produced with the RIBRAS (Radioactive Ion Beams in Brazil) system [16, 21, 28, and 29]. Elastic scattering angular distributions and the corresponding total reaction cross-sections were available in the literature for one energy (E_{lab} = 26 MeV) for the ^{8}Li + ^{51}V system [29] and two energies (14 MeV and 27 MeV) [18, 32] for the ^{8}Li + ^{9}Be system. As there are large uncertainties in the total cross-sections derived from the elastic scattering of radioactive nuclei, it is important to obtain more data to be able to include these systems in the systematic. The description of the production of radioactive ion beams using the RIBRAS facility has been discussed elsewhere [16, 21, 28, and 29]. The ^{8}Li radioactive ion beam was produced using a primary neutron transfer reaction ^{9}Be (^{7}Li, ^{8}Li). The thickness of the primary target ^{9}Be is of 12 mg/cm^{2}, which is mounted in a scattering chamber just before the first solenoid. The primary beam ^{7}Li was accelerated with a typical beam intensity of 200 nAe, measured by using an electron-suppressed Faraday cup, constituted by an isolated tungsten rod that stops all the particles in the angular region from 0 to 2 degrees and where the charges of the primary beam were integrated. A current integrator is used to measure the total charge incident on the primary target throughout the run.

The secondary beam produced from the primary reaction is collected and focused in the scattering chamber by using a superconducting solenoid of the RIBRAS facility. The particles with different magnetic rigidity were stopped from reaching the scattering chamber after the solenoid using a system of blocks and collimators. The average intensity of the secondary beam ^{8}Li at the scattering chamber was around 5×10^{4} pps, which is calculated by assuming pure Rutherford scattering of the ^{8}Li on the gold target. Even though some contaminants of ^{4}He, ^{6}He and ^{7}Li were present in the secondary beam, they did not produce reaction products similar to the ones from our reaction. The ^{8}Li laboratory energy was 19.6 MeV for the ^{9}Be target, and 18.5 MeV for the ^{51}V target. The measurements for the two systems were performed in subsequent runs. The elastic scattered reaction products with ^{8}Li particles were detected by an array of four Si surface barrier ΔE-E telescopes in an angular range of 15–35 degrees in the laboratory system, in 5 degree steps mounted on the rotating plate of the chamber. The thickness of ΔE and E detectors was 25 μm and 1mm, respectively, both having an area of 300 mm^2. Rectangular collimators were also used before the detector telescopes which subtended an angle of 12 msr for the definition of solid angles and to avoid any scattered particles from the slits. The targets were mounted at the center of the scattering chamber. The secondary targets used were self-supporting, pure ^{9}Be, ^{51}V targets of thickness 1.4 mg/cm^2 and 5 mg/cm^2, respectively. A gold target of thickness 300 $\mu g/cm^2$ was also used. The elastic scattering of ^{8}Li on this gold target was measured in all runs at different angles and used to obtain the overall normalization.

Since the cross-sections in the angular interval covered by these detectors could vary up to one order of magnitude, the average detection angle was determined by Monte Carlo simulations, which took into account the collimator size in front of the detectors, the secondary-beam spot size on the secondary target (4 mm), the secondary-beam divergence and the angular distribution in the range of the detector aperture (Rutherford on gold and calculated in an iterative way for the ^{9}Be target). This correction is important for the most forward angles. The effective angular aperture of ±3.2 degrees was calculated with a Monte Carlo simulation. Reaction products were identified using a two-dimensional ΔE-E total plot. Fig. 5.5 shows a typical 2D particle identification [C (Z, M) × E_{total}] spectrum for the ^{8}Li on ^{9}Be experiment at 19.6 MeV. Here, the particle identification
constant, C (Z,M), is given by:

$$C\ (Z, M) = (E_{total})^b - (E_{total} - \Delta E)^b\ [33], \qquad (5.1)$$

where: $E_{total} = \Delta E + E_{residual}$
and b = 1.70 for these light particles.

In this plot, the ^{8}Li scattered beam particles and the ^{4,6}He beam contaminants are shown.

The secondary-beam energies were calculated by energy losses and confirmed by the energy measurement in the Si telescope, calibrated with α-particles from a radioactive ^{241}Am source and elastically scattered secondary beams. The FWHM of the elastic peak in the energy spectrum was about 400 keV. The ratios of elastic scattering angular distributions to the Rutherford scattering for the ^{8}Li + ^{9}Be, at E_{lab} = 19.6 MeV, and ^{8}Li + ^{51}V, at E_{lab} = 18.5 MeV, are shown in Figs. 5.6(a) and (b), respectively.

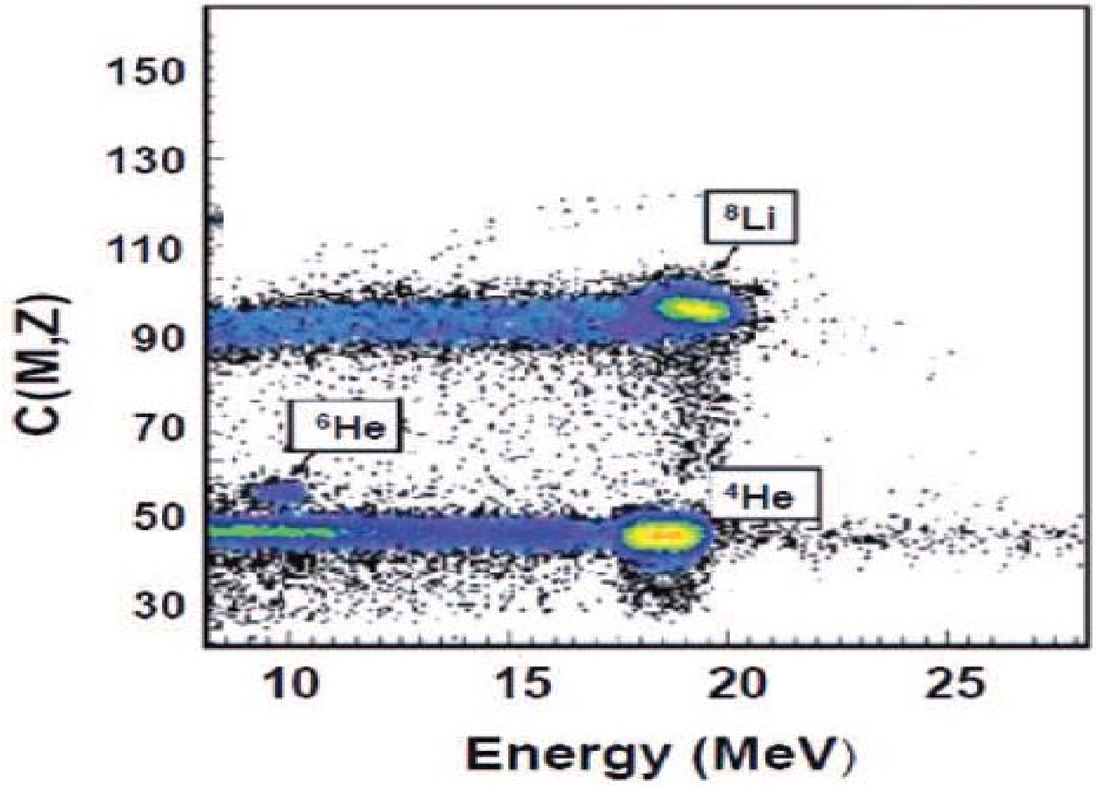

Figure 5.5. A typical 2D particle identification spectrum of the elastic scattering angular distribution obtained for the ^{8}Li + ^{9}Be system at 19.6 MeV.

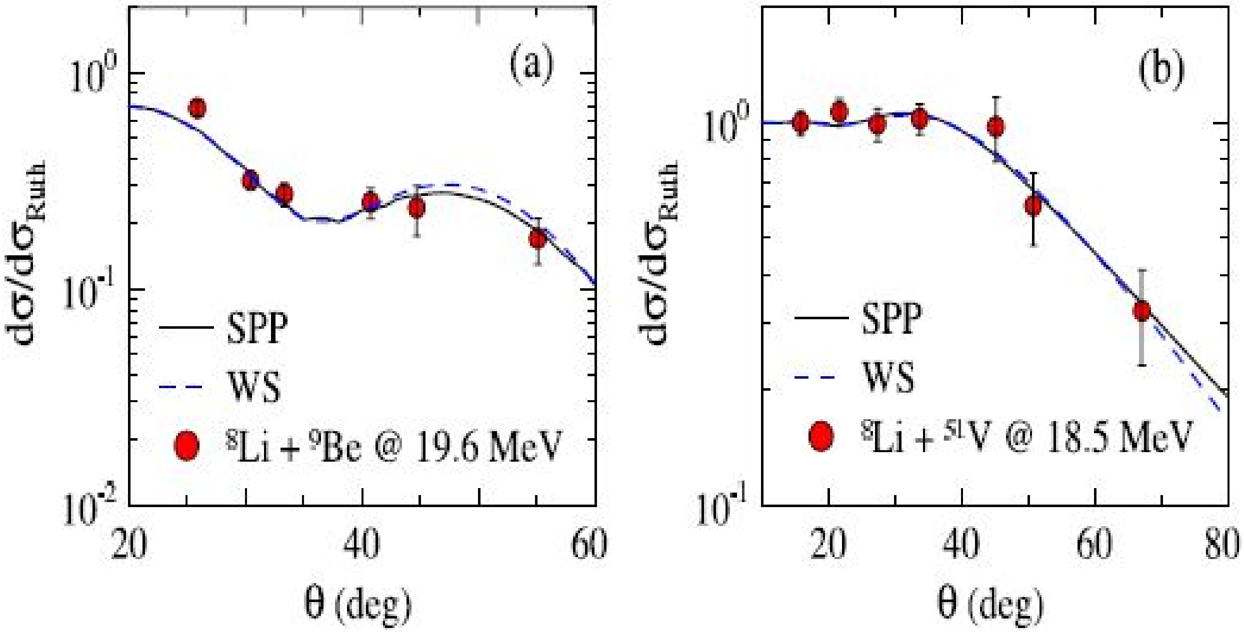

Figure 5.6. (a) Elastic scattering angular distribution for the ^{8}Li + ^{9}Be system at 19.6 MeV, and (b) Elastic scattering angular distribution for the ^{8}Li + ^{51}V system at 18.5 MeV, measured in the present work. The solid line corresponds to best fit using the Sao Paulo potential (SPP) and the dashed line using the Woods – Saxon potential (WSP) form factors. See text for details.

5.4 Optical model analysis of the elastic scattering data

The optical model (OM) analysis of elastic scattering angular-distribution data has been carried out to extract the optical potential parameters and reaction cross sections for all systems investigated in this work. The potential used for all systems, except those with the halo ^{6}He and ^{8}B, was the Sao Paulo double-folding potential (SPP) [34]. The ECIS code [35] was used for the calculations. The real potential V_N of SPP is related to the folding potential V_F by the relation,

$$V_N(R,E) = V_F(R)\exp\left(\frac{-4v^2}{c^2}\right), \tag{5.2}$$

Where; υ is the local relative velocity between the two nuclei and c is the velocity of light.

The imaginary part of the interaction is assumed to have the same shape as the real part, with one single adjustable parameter N_i related to its strength,

$$W(R, E) = N_i V_N(R, E), \tag{5.3}$$

In the present calculation the adjustable parameters taken were the strength parameters of the real and imaginary potential (N_r and N_i, respectively). It has been shown [36,37] that the analysis of elastic scattering angular distributions with SPP and with the phenomenological Woods-Saxon (WS) potential give the same results for total reaction cross-sections for tightly and no-halo weakly bound systems, but not for halo nuclei, owing to the behavior of the potential at long distances, which is incompatible with the polarizations generated by the breakup channels [38]. For this reason, for the systems involving ^{6}He and ^{8}B analyzed in the present work we used WS potentials, instead of SPP. Actually, to avoid repeating WS potential calculations for the ^{8}B+^{58}Ni system we took the reaction cross-section reported earlier [39] obtained by this procedure. For the ^{6}He + ^{51}V system, only the depths of the real and imaginary potentials were let to vary freely in the fit procedure. The reduced radii were fixed in 1.2 fm for both the real and imaginary part of the potential and its diffuseness was taken equal to 0.7 fm and 0.9 fm, respectively. Due to its intrinsic ambiguities, other optical potential parameters would give the same results. We chose a larger diffuseness for the imaginary potential to account for the halo structure of the ^{6}He projectile.

The fits of the elastic scattering data measured in the present work are shown in Fig. 5.6. The derived total reaction cross-sections and barrier parameters predicted by the SPP for all the systems investigated are shown in tables 5.2 and 5.3. The only exceptions are the reaction cross section involving halo projectiles (^{6}He and ^{8}B), for which the cross-sections were obtained using the WS optical potentials, as mentioned above. For the other systems, tests were performed using both types of potentials (as shown in Figs. 5.6(a) and (b) for the data reported in this work), and they lead to similar total reaction cross-sections. One can notice in tables 5.2 and 5.3 that the χ^2/n for ^{8}Li + ^{9}Be is larger than for the ^{8}Li + ^{51}V system. This is due to the fact that the cross-section at 15° for the ^{8}Li + ^{9}Be system (which has a small error) is larger than the calculated results. On the other hand, the calculation agrees well with the experimental data at forward angles for the ^{8}Li + ^{51}V system thereby giving rise to a small χ^2/n value.

Table 5.2. Barrier parameters obtained from the Sao Paulo potential (SPP) and derived total reaction cross-sections for the systems investigated in the present work. The cross-sections obtained from data measured in the present work are in bold.

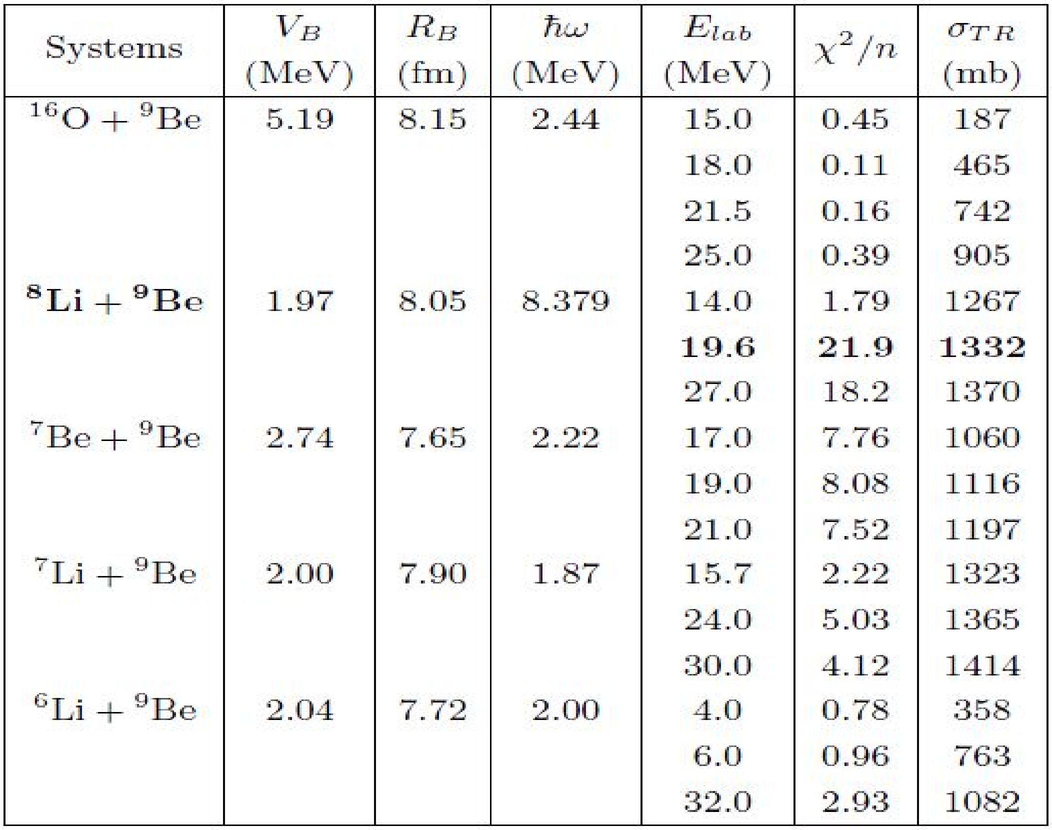

Systems	V_B (MeV)	R_B (fm)	$\hbar\omega$ (MeV)	E_{lab} (MeV)	χ^2/n	σ_{TR} (mb)
$^{16}O + {}^9Be$	5.19	8.15	2.44	15.0	0.45	187
				18.0	0.11	465
				21.5	0.16	742
				25.0	0.39	905
$^{8}Li + {}^9Be$	1.97	8.05	8.379	14.0	1.79	1267
				19.6	**21.9**	**1332**
				27.0	18.2	1370
$^{7}Be + {}^9Be$	2.74	7.65	2.22	17.0	7.76	1060
				19.0	8.08	1116
				21.0	7.52	1197
$^{7}Li + {}^9Be$	2.00	7.90	1.87	15.7	2.22	1323
				24.0	5.03	1365
				30.0	4.12	1414
$^{6}Li + {}^9Be$	2.04	7.72	2.00	4.0	0.78	358
				6.0	0.96	763
				32.0	2.93	1082

Table 5.3. Barrier parameters obtained from the Sao Paulo potential (SPP) and derived total reaction cross-sections for the systems investigated in the present work. The cross-sections obtained from data measured in the present work are in bold.

Systems	V_B (MeV)	R_B (fm)	$\hbar\omega$ (MeV)	E_{lab} (MeV)	χ^2/n	σ_{TR} (mb)
^{4}He + ^{51}V	7.49	8.20	3.93	23.2	1.0	1259
^{4}He + ^{56}Fe	8.38	8.30	4.08	25.0	28.0	1336
^{6}He + ^{51}V	6.61	9.25	2.72	15.4	0.9	1901
				23.0	0.4	2474
^{4}He + ^{64}Zn	9.50	8.45	4.31	13.0	0.8	585
				25.0	22.2	1365
^{6}Li + ^{58}Ni	12.37	9.00	3.67	11.21	0.6	19
				12.13	0.1	40
				13.04	0.1	109
				14.04	0.3	225
				9.85	0.5	1.1
^{7}Be + ^{58}Ni	16.59	8.95	3.91	15.09	0.1	21
				17.13	0.1	78
				18.53	0.1	193
				19.93	0.1	333
				21.43	0.1	499
^{8}B + ^{58}Ni	20.80	8.92	4.09	20.7	0.15	198
				23.4	0.58	363
				25.3	0.33	512
				27.2	0.41	812
				29.3	0.13	1005
^{8}Li + ^{51}V	9.93	9.25	2.90	**18.5**	**0.3**	**975**
				26.0	1.5	1984

5.5 Reduction procedure of total reaction cross section

In order to perform a systematic study of total reaction cross-sections with different weakly bound projectiles with several targets, it is necessary to compare the cross sections for systems with different Coulomb barriers. For this purpose, it is necessary to suppress the differences arising from the size and charges of the systems. This can be done in different ways. The two most frequently used reduction procedures are to normalize the collision energy with respect to the barrier height and to divide the cross-section by its geometrical value, i.e., to plot $\sigma_R/\pi R^2B$ against $E_{c.m.}-V_B$ or $E_{c.m.}/V_B$, where R_B and V_B are the s-wave barrier radius and height respectively, and should be evaluated using a realistic treatment of the optical potential similar to the folding model. However, this procedure does not consider the important influence of the barrier curvature at the sub-barrier energies [20]. It has been pointed out [19] that when weakly bound projectile nuclei are involved, care should be taken in order to preserve the static effects arising from the low breakup energy of the projectile. So, the reduction method removes the dependence on the masses and charges of the collision partners but not specific features of the projectile density. The proposed reduction method [19] is to plot $\sigma_R/(A_p^{1/3} + A_t^{1/3})^2$ versus $E_{c.m.}(A_p^{1/3} + A_t^{1/3})/Z_pZ_t$. This method has been extensively used to investigate the role of breakup of weakly bound nuclei on the fusion and reaction cross-sections for a variety of systems (see, for example, refs. [14, 15, 21, 39–47]).

However, it was recently pointed out [20] that the above-mentioned reduction procedures fail to remove appropriately the static effects on the fusion reactions of different systems. In the newly proposed methodology [20], this is achieved. This methodology was later extended to be used with total reaction cross-sections [13]. The procedure takes into account not only the height and radius of the Coulomb barrier, but also its curvature represented by the quantity $\hbar\omega$. The collision energy and the cross-section are reduced, for fusion cross-sections, as $F_F(x) = (2E_{c.m.}/\hbar\omega R^2B)\sigma_F$ and $x = (E_{c.m.} - V_B)\ \hbar\omega$. Similarly, for total reaction cross sections one uses $F_{TR}(x) = (2E_{c.m.}/\hbar\omega R^2B)\ \sigma_{TR}$. The barrier parameters are extracted from the optical potential used. $F_F(x)$ was called fusion function and $F_{TR}(x)$ was called total reaction function. It has been shown [20] that this fusion function is system independent when σ_F is accurately described by Wong's formula [48]. In this case F(x) becomes $F(x) \rightarrow F_0(x) = \ln[1 + \exp(2\pi x)]$. Note that $F_0(x)$ depends exclusively on the dimensionless variable *x*. It is a universal function which is the same for any system. For this reason it is called the Universal Fusion Function (UFF), and it can be used as a benchmark to which renormalized data should be compared [20].

5.6 Results and discussion of analysis of total reaction by different reduction procedures

In Fig. 5.7 we compare total reaction cross-sections for the ^{8}Li + ^{9}Be system and the available total reaction cross-sections for the ^{6,7}Li + ^{9}Be [49,50], ^{7}Be + ^{9}Be [51], ^{16}O + ^{9}Be [52] systems using the two above-mentioned reduction methods. We notice that for all systems the target is a weakly bound nucleus and the projectiles are either a tightly bound nucleus or a weakly bound one but not a halo nucleus. The total reaction cross-sections are in the energy region above the Coulomb barrier. In Fig. 5.7(b) we also show the UFF, as a reference curve. One can observe that the results are similar for all the systems when one reduces the data by both methods. So, both reduction methods lead to the same conclusions. The radioactive ^{8}Li projectile has the same reduced total reaction cross section as the stable ^{6}Li isotope. One can notice that the total reaction cross-section for the tightly bound ^{16}O projectile is slightly smaller than for the other weakly bound systems in Fig. 5.8(a), but not in Fig. 5.7(b), where all systems have total reaction cross-sections similar to the UFF. Similar results are present in refs. [13,21] for a similar study with the ^{27}Al target.

In Fig. 5.8 we compare total reaction cross-sections for the ^{8}Li + ^{51}V system and the available total reaction cross-sections for the ^{4}He + ^{51}V [16], ^{6}He + ^{51}V [39], ^{4}He + ^{56}Fe [53], ^{4}He + ^{64}Zn [53–55], ^{6}Li + ^{58}Ni [39], ^{7}Be + ^{58}Ni [39], ^{8}B + ^{58}Ni [39] and ^{16}O + ^{64}Zn [56] systems using the same two reduction methods. We notice that the projectiles are either a tightly bound nucleus or a weakly bound one, including the neutron halo ^{6}He and the proton halo ^{8}B nuclei. Reactions with the halo projectiles ^{6}He and ^{8}B have total reaction cross-sections higher than the others, independently whether they are tightly or weakly bound nuclei, by both reduction methods. ^{8}Li has the same behavior as the stable ^{7}Li isotope. Once again, the conclusions are the same from both reduction methods, although the ^{16}O projectile shows smaller total reaction cross-section by the method of Fig. 5.8(a). These conclusions are consistent with the ones obtained in ref. [13] for heavier systems. In that work, only total reaction functions induced by neutron halo (^{6}He) and proton halo (^{8}B) projectiles were larger than for those induced by weakly or tightly bound nuclei.

For the data analyzed in the present work, both reduction procedures lead to the same conclusions. However, one has to have in mind that the systems investigated here are not so different having similar product of the projectile and target charges. By the reduction method of ref. [19] there is a trend that heavier projectiles on the same target have smaller total reaction cross-sections, as one can observe in Figs. 5.8(a) and 5.9(a) for the ^{16}O projectile. It is still a matter of further investigation which is the best way to reduce total reaction cross-section data.

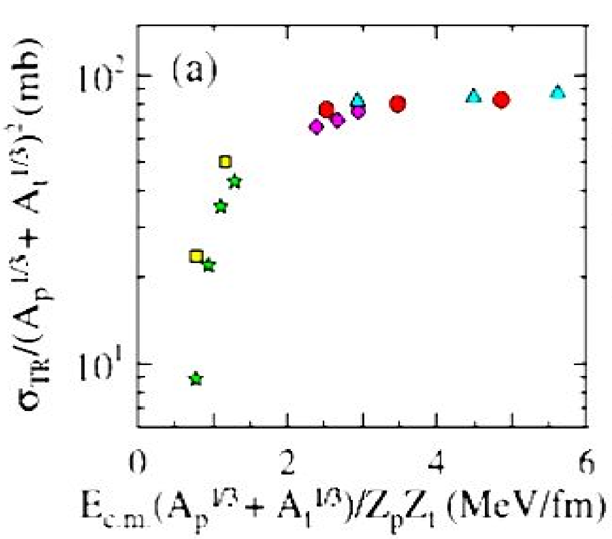

Figure 5.7. Total reaction cross-sections for systems with different projectiles and the same ^{9}Be target, reduced by the two different reduction methods described in the text. The curve in (b) is the universal fusion function.

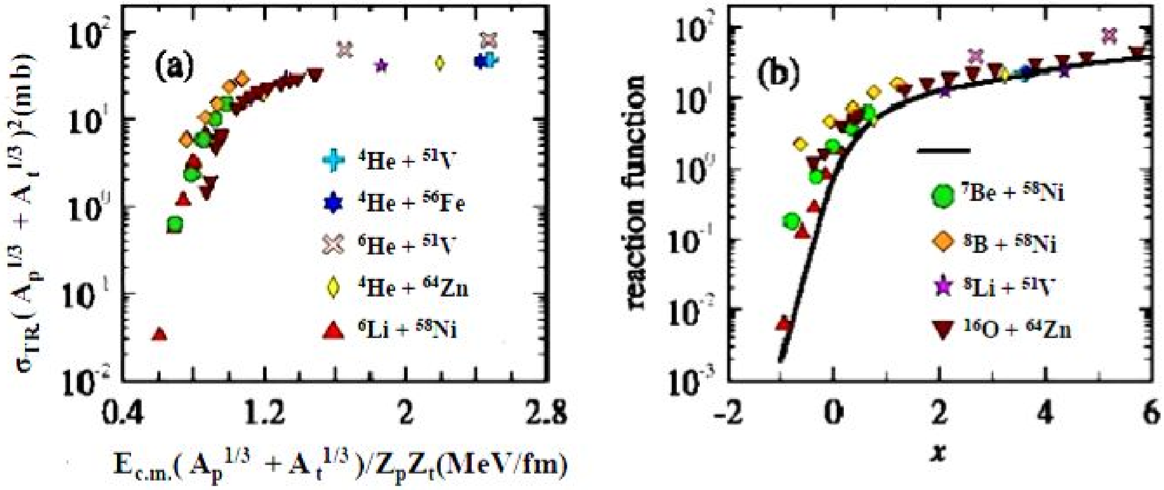

Figure 5.8. Total reaction cross-sections for systems with different projectiles and targets from A = 51 to 64, reduced by the two different reduction methods described in the text. The curve in (b) is the universal fusion function.

5.7 Conclusions

This chapter reports the new measurement of elastic scattering cross-section for ^{8}Li + ^{9}Be and ^{8}Li + ^{51}V systems at 19.6 MeV and 18.5 MeV, respectively, using the radioactive beam facility RIBRAS at Sao Paulo, Brazil. Analyses were performed for previously reported data for these systems and for many other light systems. The double-folding Sao Paulo potential was used in the analysis of all systems, except for the ones with halo nuclei. In these cases, χ^2 fits and data analysis were performed using Wood-Saxon shape optical potentials. Tests were performed by using both types of potentials for non-halo systems, and they lead to similar total reaction cross-sections, which were extracted from the optical model fits. The total reaction cross-sections for all systems, and by the two reducing methods used, were found to be similar, irrespective of the projectile being tightly or weakly bound, stable or radioactive, except when halo nuclei were present. In this situation, the total reaction sections were larger than for the others.

References

[1] R. Rafiei et al., Phys. Rev. C **81**, 024601 (2010).

[2] M. Dasgupta et al., Phys. Rev. C **81**, 024608 (2010).

[3] N. Keeley et al., Prog. Part. Nucl. Phys. C **63**, 397 (2009).

[4] M. Zadro et al., Phys. Rev. C **80**, 064610 (2009).

[5] Florin Carstoin et al., Phys. Rev. C **70**, 054610 (2004).

[6] P.R.S. Gomes et al., Phys. Rev. C **79**, 027606 (2009).

[7] L.F. Canto et al., Nucl. Phys. A **821**, 51 (2009).

[8] H. Kumawat et al., Phys. Rev. C **78**, 044617 (2008).

[9] C. Beck et al., Phys. Rev. C **67**, 054602 (2003).

[10] V. Guimarães et al., Phys. Rev. C **75**, 054602 (2007).

[11] R. Kanungo et al., Phys. Lett. B **660**, 26 (2008).

[12] H.B. Jeppesen et al., Phys. Lett. B **642**, 449 (2006).

[13] J.M.B. Shorto et al., Phys. Lett. B **678**, 77 (2009).

[14] J.J. Kolata, E.F. Aguilera, Phys. Rev. C **79**, 027603 (2009).

[15] E.F. Aguilera et al., Phys. Rev. C **80**, 044605 (2009).

[16] A. Lépine-Szily, R. Lichtenthäler, Nucl. Phys. A **787**, 94c (2007).

[17] F.D. Becchetti et al., Phys. Rev. C **40**, R1104 (1989).

[18] O. Camargo et al., Phys. Rev. C **78**, 034605 (2008).

[19] P.R.S. Gomes et al., Phys. Rev. C **71**, 017601 (2005).

[20] L.F. Canto et al., J. Phys. G: Nucl. Part. Phys. **36**, 015109 (2009).

[21] E.A. Benjamim et al., Phys. Lett. B **647**, 30 (2007).

[22] R. Lichtenthäler et al., Brasilian Journal of Physics, Vol. 33, no. 2, (2003).

[23] R. Lichtenthäler et al., Nucl. Inst. & Meth. in Phys. Res. A **505**, 612 – 615, (2003).

[24] M.Y. Lee, Ph. D. Thesis, University of Michigan (2002).

[25] XIII J.A. Swieca Summer School on Experimental Nuclear Physics, Pelletron – IFUSP (2004).

[26] H. Geissel, G. Munzenberg and K. Risager, Ann. Rev. Nuclei Sci. **45**, 163 (1995).

[27] W.A. Fowler, Experimental and Theoretical Nuclear Astrophysics: the quest for the origin of the elements, Reviews of Modern Physics **56**, no.2, pt. 1, 149 – 179 (1984).

[28] R. Lichtenthäler et al., Eur. Phys. J. A **25**, s01, 733 (2005).

[29] R. Lichtenthäler et al., AIP Conf. Proc. **1139**, 76 (2009).

[30] S. Mukherjee, N. N. Deshmukh et al., Eur. Phys. J. A **45**, 23 – 28 (2010).

[31] F. D. Becchetti et al., Nucl. Inst. & Meth. in Phys. Res. B **56/57**, 554 (1991).

[32] F. D. Becchetti et al., Phys. Rev. C **48**, 308 (1993).

[33] G.F. Knoll, Radiation Detection and Measurement (Wiley & Sons, New York, 1989) p. 380.

[34] L.C. Chamon et al., Phys. Rev. C **66**, 014610 (2002).

[35] J. Raynal, Phys. Rev. C **23**, 2571 (1981).

[36] J.M. Figueira et al., Phys. Rev. C **73**, 054603 (2006).

[37] J.M. Figueira et al., Phys. Rev. C **75**, 017602 (2007).

[38] A.R. Garcia et al., Nucl. Phys. A **806**, 146 (2008).

[39] E.F. Aguilera et al., Phys. Rev. C **79**, 021601(R) (2009).

[40] A. Barioni et al., Phys. Rev. C **80**, 034617 (2009).

[41] F.A. Souza et al., Nucl. Phys. A **821**, 36 (2009).

[42] U. Gupta et al., Nucl. Phys. A **811**, 77 (2008).

[43] A. Di Pietro, Eur. Phys. J. ST **150**, 15 (2007).

[44] M. Sinha et al., Phys. Rev. C **76**, 027603 (2007).

[45] K. Kalita et al., Phys. Rev. C **73**, 024609 (2006).

[46] E.F. Aguilera, J.J. Kolata, L. Acosta, Phys. Rev. C **81**, 011604(R) (2010).

[47] M. Mazzocco et al., Nucl. Phys. A **834**, 488c (2010).

[48] C.Y. Wong, Phys. Rev. Lett. **31**, 766 (1973).

[49] J. Cook, K.W. Kemper, Phys. Rev. C **31**, 1745 (1985).

[50] P.L. Von Behren et al., Phys. Rev. C **10**, 550 (1974).

[51] S. Verma et al., Eur. Phys. J. ST **150**, 75 (2007).

[52] Z.E. Switkowski et al., Nucl. Phys. A **289**, 236 (1977).

[53] F. Ballester, E. Casal, J.B.A. England, Nucl. Phys. A **501**, 301 (1989).

[54] A. Di Pietro et al., Phys. Rev. C **69**, 044613 (2004).

[55] F. Ballester, E. Casal, J.B.A. England, Nucl. Phys. A **490**, 245 (1988).

[56] C. Tenreiro et al., Phys. Rev. C **53**, 2870 (1996).